12. ANTHROPOGENIC FORCINGS AND ASSOCIATED CHANGES IN FIRE RISK IN WESTERN NORTH AMERICA AND AUSTRALIA DURING 2015/16

Simon F. B. Tett, Alexander Falk, Megan Rogers, Fiona Spuler, Calum Turner, Joshua Wainwright, Oscar Dimdore-Miles, Sam Knight, Nicolas Freychet, Michael J. Mineter, and Caroline E. R. Lehmann

Extreme vapor pressure deficits (VPD) have been associated with enhanced wildfire risk. Using one model, we found for 2015/16 that human influences quintupled the risk of extreme VPD for western North America and increased the risk for extratropical Australia.

Introduction. In 2016, about 3.6 million hectares of land burned in the United States and Canada (NIFC 2017; NFD 2017). In Canada, a wildfire southwest of Fort McMurray, Alberta, caused the largest wildfire evacuation in Alberta's history and destroyed 2400 homes in 2016 (McConnell 2016). Abatzoglou and Williams (2016; AP16 from hereon) showed that anthropogenic climate change has increased forest fire activity in the western United States. This raises the question if anthropogenic forcing are increasing the risk of devastating events outside this region such as the Canadian Fort McMurray fire.

During the Australian summer of 2015/16, the country experienced high numbers of bushfires: the southwest and southeast of the country were most affected with more than 100000 hectares of vegetation burned in Tasmania (ABC News 2016a). Over the course of this summer, 408 residential and 500 non-residential buildings were destroyed nationwide. This fire season was moderately destructive with insured losses of about AUD $350 million (ABC News 2016b).

AP16 found for the western United States a strong link between the spring–summer vapor pressure deficit (VPD) and the annual burned area. In this paper, we build on this work using monthly average VPD as a proxy for fire risk during the summer of 2016 for extratropical Australia (October–February) and western North America (May–August) though

this link has not been directly established for either region. VPD is an absolute measure of the state of atmospheric moisture, specifically the difference between the saturation vapor pressure and the actual vapor pressure of the atmosphere (Seagar et al. 2015). Changes in VPD are associated with the drying of both live vegetation and litter fuels, and it is only when vegetation and litter fuels are sufficiently dry that fires can both ignite and spread (Bradstock 2010).

Methods. To estimate the effect of anthropogenic climate change on VPD in western North America and extratropical Australia, we compared three different ensembles of the HadAM3P atmosphere-only model (Massey et al. 2015), which has a resolution of 1.875° × 1.25°, with each other and the ERA-Interim (ERAI) reanalysis (Dee et al. 2011). The ensembles are:

- **Hist15–16**: Driven by observed sea surface temperatures (SST), sea ice coverage (SIC) as well as current concentrations of greenhouse gases and estimates of aerosol emissions (updated from Tett et al. 2013).
- **Nat15–16**: Driven by SST, SIC, greenhouse gases, and aerosol emissions as they are estimated to have been without human induced climate change with natural SST (Fig. ES12.1a) and SIC conditions described in the online supplement.
- **Historical:** Ensemble of 5 continuous simulations from December 1959 to November 2009 described by Tett et al. (2013).

Both Hist15–16 and Nat15–16 have 24 members, each using slightly different initial conditions, starting in December 2014 and ending in August 2016. We analyze the 12-month period September 2015 to

August 2016. VPD is defined as (Seager et al. 2015; Wallace and Hobbs 2006):

$$VPD = e_s - e \quad \& \quad e_s = \frac{e}{RH}$$

and, neglecting moisture mass in the atmosphere, can be rewritten as:

$$VPD = \frac{M_{dry\,air}}{M_{H_2O}} q\,p^* \left(\frac{1}{RH} - 1 \right) \qquad \text{Eq. (1)}$$

where $e(e_s)$ is the (saturated) vapor pressure, q the specific humidity, p^* the surface pressure, and RH the relative humidity near the surface.

We computed VPD in the HadAM3P simulations and ERAI reanalysis using Eq. (1) applied to gridded monthly mean data neglecting nonlinearity. For HadAM3P, q and RH were 1.5 meter values while for ERAI we interpolated q and RH from monthly mean pressure level data to the surface. We use as a reference period the 30 years 01 December 1979–30 November 2009 and VPD, q_{sat} (q/RH), q, and p^* were converted

to anomalies against this period from the Historical or ERAI values.

The western North America (WNA) region was defined as in Giorgi and Francisco (2000; GF00), while we defined an extratropical Australian region (extAUS) as the GF00 AUS region south of 23.5°S. Fire does not occur in all places in the regions, so we defined a fire-mask to keep locations in our analysis where fire occurs. This mask was constructed from the MODIS CMG dataset using *Aqua* satellite measurements (Giglio et al. 2009) for 2003–16. Each $0.5° \times 0.5°$ grid box and climatological month, was defined as a fire grid box if the fraction of pixels with fire detected for 2003–16 was greater than 10^{-5} (Figs. ES12.1b–e show regions and fraction of fire pixels for January and July). The 10^{-5} is arbitrary and corresponds to roughly one detected fire pixel per month. Simulated (and reanalysis) VPD, q, RH, q_{sat} (q/RH), and p^* anomalies and normals were bilinearly interpolated to this grid from the model/reanalysis grid, data only kept at fire grid boxes, and then area
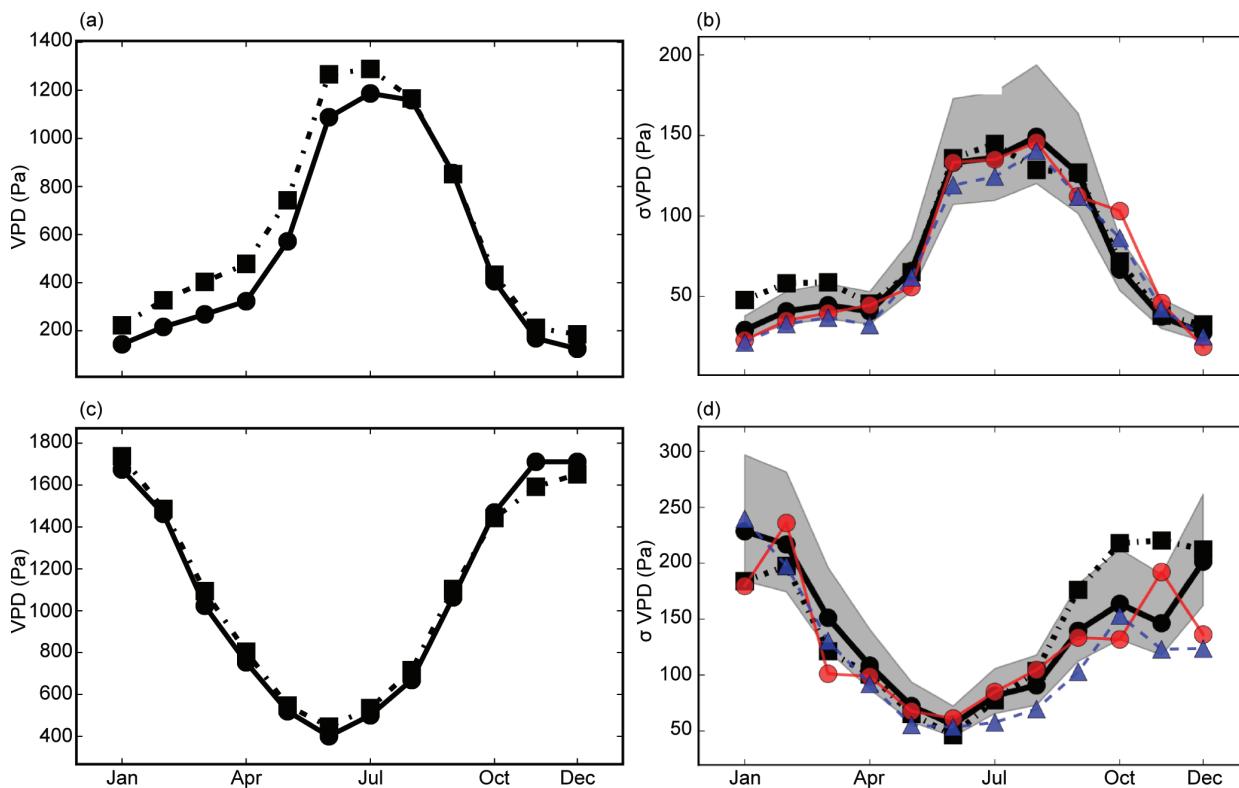

Fɪɢ. 12.1. VPD (Pa) comparison between ERAI (black dot-dashed, squares) and Historical (black lines, circles): (a),(c) 01 Dec 1979–Nov 2009 normals; (b),(d) std. dev. for WNA and extAUS, respectively. Gray shading indicates where reanalysis and Historical std. dev. are consistent (5%–95%). Std. dev for Sep 2105–Aug 2016 from Hist15–16 (red circles, lines) and Nat15–16 (blue triangles, dashed lines) are also shown in (b),(d). The x-axis on all plots shows climatological month (labels on bottom plots only).
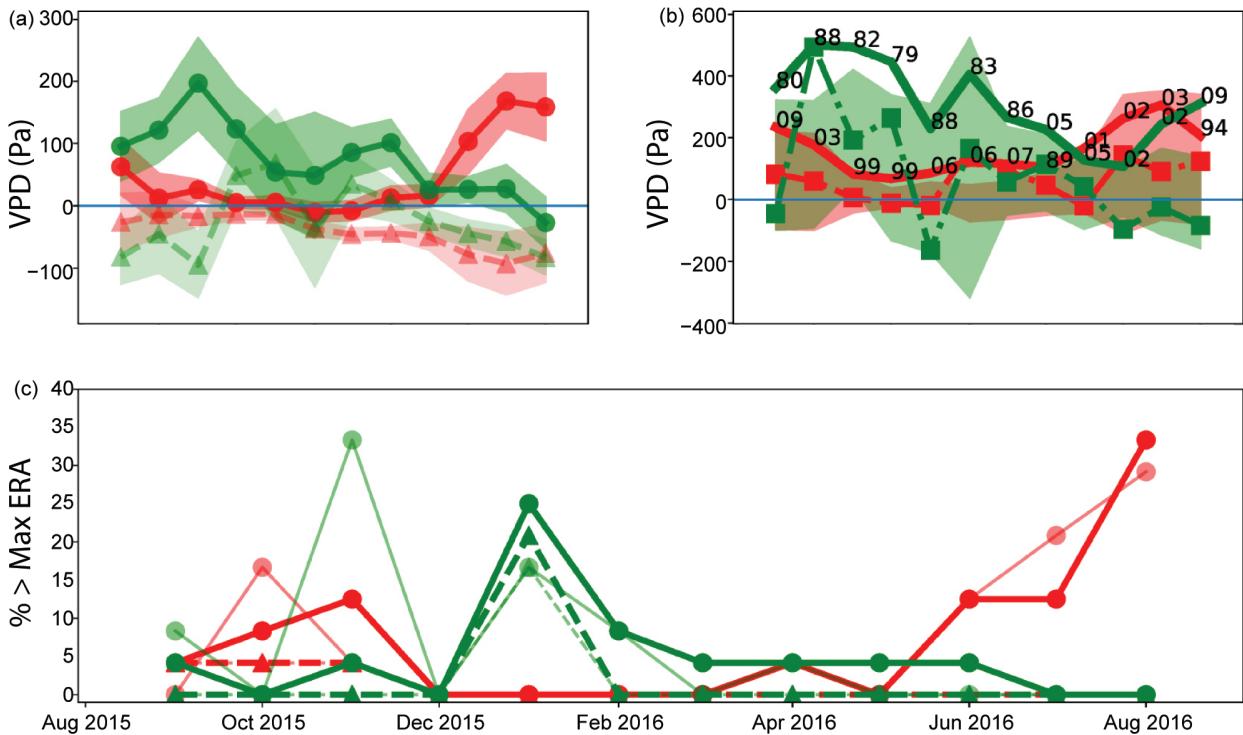
FIG. 12.2. (a) Ensemble-mean **VPD** anomalies (Pa) from Hist15–16 (circles) and Nat15–16 (triangles) for **WNA** (red) and **extAUS** (green). Shading shows ±2σ uncertainty. (b) Maximum VPD anomaly (Pa) for each climatological month [thick solid line and year (number) when max occurred] and anomaly for 15/16 (squares) from ERAI. Shading shows 5%–95% ranges from Hist15–16 ensemble with colors as (a). (c) Fraction (%) of Nat15–16 (dashed lines, triangles) and Hist15–16 (solid lines, circles) ensembles that exceeded 1979–2009 ERAI maximum VPD value for each month. Thin pale lines show same when anomalies scaled to correct for variance errors. All subplots use same common x-axis [values shown in (c)].

averaged over the two regions to produce time series. It is these time series that we subsequently analyze. Uncertainties on ensemble averages were computed by bootstrapping (Efron and Tibshirani 1994) over the ensemble members.

We define as a threshold for extreme events the ERAI maximum regional average VPD anomaly, for each calendar month, from the reference period corresponding to a one-in-30-year event. To compute the risk of exceeding this threshold we compute, for each month, the fraction of the Nat15–16 and Hist15–16 anomalies that exceed it. We test sensitivity to variance errors by scaling the Hist15–16 and Nat15–16 anomalies by the ratio of the monthly mean standard deviations from ERAI and Historical anomalies for the reference period.

Results. Model simulations are evaluated by comparing the Historical ensemble with ERAI. HadAM3P's VPD biases are small relative to the annual cycle though are negative for most of the year in WNA (Fig. 12.1a) with largest differences in June of −180 Pa. HadAM3P

VPD variance appears consistent with that of ERAI (Fig. 12.1b) though the model has significantly smaller variance than ERAI for January–March, and there is no strong evidence of an increase in variability due to human forcings.

For extAUS Historical mean, VPD is, apart from November and December, consistent with that from ERAI (Fig. 12.1c). In November and December biases peak at about +120 Pa. Variability from reanalysis and HadAM3P is broadly consistent though reanalysis variability during austral summer is generally larger than simulated in HadAM3P. For most of the year, extAUS has larger variability in Hist15–16 and Historical than in Nat15–16 (Fig. 12.1d). Mean VPD values peak in WNA in June–August while in extAUS they are largest during October–February. It is these components of the annual cycle we subsequently focus on.

We now compare ensemble means from Hist15–16 with Nat15–16. For WNA, differences between the two ensembles are significant throughout most of the year with largest differences in July and August 2016 (Fig. 12.2a). For extAUS the Hist15–16 (Nat15–16)

ensemble has positive (negative) anomalies for most of the period suggesting that human influences have increased VPD. However, during December 2015 and January 2016 Nat15–16 shows positive anomalies.

We compare the Hist15–16 ensemble anomalies with ERAI (Fig. 12.2b). For both regions Hist15–16 is broadly consistent with ERAI though extAUS in October 2015, and WNA in February 2016 are exceptions to this (Fig. 12.2b). ERAI VPD values for September 2015 to August 2016, though generally larger than Nat15–16, are not very exceptional with almost all values being smaller than the maximum 1979–2009 VPD value. Maximum ERAI anomalies occur throughout the reference period with no obviously preferred year (or decade).

We now investigate the probability, for both ensembles, of crossing the 1979–2009 threshold. In extAUS, only in January 2016 do any of the Nat15–16 members cross the ERAI threshold (Fig. 12.2c). In WNA, the threshold is exceeded once in each of September through November 2015. For extAUS, there is an approximate doubling of the probability of exceeding the thresholds for October–February with a probability of about 7% (4%) for Hist15–16 (Nat15–16). May 2016, when the Fort McMurray fires started, has near-zero anomaly for WNA in both ensembles and reanalysis suggesting that this event was not strongly linked to continental scale VPD changes, and no ensemble members cross the 30-year threshold (Fig. 12.2c) during this month. However, during June 16–August 16, we find several extreme VPD values in the Hist15–16 ensemble, and no such events in the Nat15–16 ensemble (Fig. 12.2c). The average probability of crossing the threshold during this period is 19%. Making a relative risk estimate is difficult when the probability of events in the natural world are small. Being very conservative we assume, with 24 ensemble members, that the probability of crossing the threshold in Nat15–16 is 4% (1/24) giving a risk ratio of about 5, though larger values are possible.

We tested the sensitivity of these results to correcting for variance errors and found little sensitivity in WNA, but the risk for extAUS changed to 12% (3%) for Hist15–16 (Nat15–16) suggesting a risk ratio of about 4. Being conservative and taking the risk of 1:30 events for Nat15–16 as 4% then the risk of extreme VPD events, in extAUS, has increased by 2–3 times.

Our estimation of risk ratios is dependent on HadAM3P and the boundary conditions used. HadAM3P compares well with the ERAI VPD climatology (Fig. 12.1a) and the reanalysis values for September 2015–August 2016 are largely contained within the Hist15–16 ensemble (Fig. 12.2a). We decompose the changes in VPD into changes in saturated humidity, surface pressure, relative humidity, and residual effects (see online supplement and Fig. ES12.2). We find that changes in saturated humidity (likely dominated by changes in temperature) and relative humidity (likely model sensitive) are the dominant drivers of VPD in both regions. In WNA, changes in q_{sat} make the largest contribution with a small enhancement by reductions in RH. In contrast, for extAUS changes in RH offset changes in q_{sat} suggesting some model sensitivity in that region. Overall, we conclude that for WNA that human influences have very considerably increased the risk of extreme VPD values in June–August 2016, though not for the Fort McMurray fire period in May. For extratropical Australia, we find a weaker human influence with a doubling of the risk of extreme VPD. Assuming wildfire in extAUS and WNA, like in the western United States, is related to VPD then human influences have considerably increased the risk of one-in-30-year wildfire events.

REFERENCES

ABC News, 2016a: *Major bushfires in Australia in 2015-2016 summer: Before and after.* ABC News [Australia] website, accessed 29 March 2017. [Available online at www.abc.net.au/news/2016-03-15/satellite-pictures-reveal-scale-of-summersbushfire-destruction/7232594.]

——, 2016b: *Catastrophic Summer events cost insurers more than $550 million,Insurance Council of Australia says*, ABC News [Australia] website, accessed 29 March 2017. [Available online at www.abc.net.au/news/2016-03-25/catastrophes-summer-costs-insurance-companies-more-than-550m/7276564.]

Abatzoglou, J. T., and A. P. Williams, 2016: Impact of anthropogenic climate change on wildfire across western US forests. *Proc. Natl. Acad. Sci. USA*, **113**, 11,770–11,775, doi:10.1073/pnas.1607171113.

Bradstock, R. A., 2010: A biogeographic model of fire regimes in Australia: Current and future implications. *Global Ecol. Biogeogr.*, **19**, 145–158, doi:10.1111/j.1466-8238.2009.00512.x.

Dee, D. P., and Coauthors, 2011: The ERA-Interim reanalysis: Configuration and performance of the data assimilation system. *Quart. J. Roy. Meteor. Soc.*, **137**, 553–597, doi:10.1002/qj.828.

Efron, B., and R. J. Tibshirani, 1994: *An Introduction to the Bootstrap.* CRC press, 456 pp.

Giglio, L., T. Loboda, D. P. Roy, B. Quayle, and C. O. Justice, 2009: An active-fire based burned area mapping algorithm for the MODIS sensor. *Remote Sens. Environ.*, 113, 408–420, doi:10.1016/j.rse.2008.10.006.

Giorgi, F., and R. Francisco, 2000: Uncertainties in regional climate change prediction: A regional analysis of ensemble simulations with the HADCM2 coupled AOGCM. *Climate Dyn.*, **16**, 169–192, doi:10.1007/PL00013733.

Massey, N., and Coauthors, 2015: weather@home—development and validation of a very large ensemble modelling system for probabilistic event attribution. *Quart. J. Roy. Meteor. Soc.*, **141**, 1528–1545, doi:10.1002/qj.2455.

McConnell, R., 2016: Fort McMurray is 'still alive,' fire chief says — but safety concerns linger. Canadian Broadcasting Corporation News, webstory. [Available at www.cbc.ca/news/canada/edmonton/fort-mcmurray-tour-notley-media-1.3572982, Date accessed 2017-03-29.]

NFD, 2017: National forest and forest management statistics. National Forestry Database [Canada], accessed 30 March 2017. [Available online at http://nfdp.ccfm.org/index_e.php.]

NIFC, [2017]: Total wildland fires and acres. National Interagency Fire Center [U.S.], accessed 29 March 2017. [Available at www.nifc.gov/fireInfo/fireInfo_stats_totalFires.html.]

Seager, R., A. Hooks, A. P. Williams, B. Cook, J. Nakamura, and N. Henderson, 2015: Climatology, variability, and trends in the U.S. vapor pressure deficit, an important fire-related meteorological quantity. *J. Appl. Meteor. Climatol.*, **54**, 1121–1141, doi:10.1175/JAMC-D-14-0321.1.

Tett, S. F. B., K. Deans, E. Mazza and J. Mollard, 2013: Are recent wet northwestern European summers a response to sea ice retreat? [in "Explaining Extreme Events of 2012 from a Climate Perspective"]. *Bull. Amer. Meteor. Soc.*, **94** (9), S32–S35.

Wallace, J., and P. Hobbs, 2006: *Atmospheric Science: An Introductory Survey.* 2nd ed. Academic Press, 483 pp.